Program Digest, 2019 IEEE International Ultrasonics Symposium (IUS)
Glasgow, Scotland, October 6-9, 2019

Wave propagation in an acoustic waveguide for ultrasonic phased arrays

Matthias Rutsch[1], Axel Jäger[1], Alexander Unger[1], Thomas Kaindl[2], and Mario Kupnik[1]
[1]Technische Universität Darmstadt, Germany,
[2]Pepperl+Fuchs AG, Mannheim, Germany.

***Abstract*—We present a simulation of an acoustic waveguide array consisting of 64 circular-shaped ducts with equal lengths. The waveguide reduces the acoustic aperture to an effective element pitch of half lambda. In order to optimize the waveguide geometry regarding sound pressure level and time delay between the channels and directivity, we use the acoustic boundary element method of COMSOL Muliphysics 5.4. The main objective for this work, is to simulate and measure the directivity pattern in the far field region based on the wave propagation inside the waveguide in order to extend our previous simulation of ultrasonic phased arrays. The complexity of the model was reduced using two symmetry planes. The wave propagation is calculated in the frequency domain based on the Helmholtz equation. A finite-sized rigid baffle at the acoustic aperture side of the array, identical to the one used in the measurements, is included. Our model allows visualizing the wave propagation in our waveguide. As the geometry intended, all waveguides emit the ultrasound in phase. Due to a different distribution of the normal velocity of the real transducers, the half power beam width differs only 4° and the side lobe level 3 dB compared to measurements.**

***Index Terms*—BEM, wave propagation, duct acoustics**

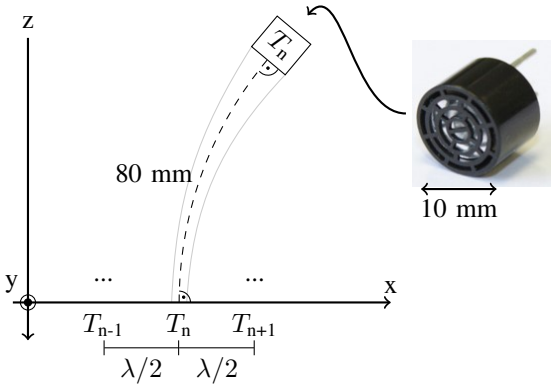

Fig. 1. The geometry of a single waveguide consisting of a tube with a tapering diameter. The centre line of the tube follows a circular arc starting perpendicular to the transducer surface and ending perpendicular to the output surface of the tube. This reduces the effective pitch to $\lambda/2$.

I. Introduction

Low frequency ultrasound between 20 kHz and 500 kHz is suitable for air coupled applications such as obstacle detection, gas flow metering, acoustic imaging or even haptic holograms. The technical properties of theses systems can be enhanced by using steerable ultrasound in order to scan an area or an entire volume of interest for a certain task. Ultrasonic phased arrays are capable of steering their acoustic main lobe via phase shifts between each individual channel, and, thus, extending the acoustic sensor capabilities for these systems [1]. The propagation direction of the array can be manipulated by electrical phase shifts of each independent transducer. In order to accomplish a high steering angle without grating lobes, a pitch of half-wavelength between the elements is required. We achieved this objective by using commercial available ultrasonic transducers and a 3D printed waveguide structure [2] - [4]. In our previous work, we characterized and simulated our acoustic system. The simulation consisted of 8×8 equidistant ideal piston transducers, positioned at our output surface of the waveguide [5]. In this work, we extend our previous simulation with the acoustic waveguide and a finite-sized rigid baffle using the boundary element method (BEM) package of COMSOL multiphysics 5.4.

Numerical methods such as finite element method (FEM) or BEM offer the possibility to calculate complex structures which can not be analytically modeled using zero or even one dimensional geometries [6]. In particular duct acoustics analytic models have geometrical restrictions such as a minor radius in comparison to the wavelength and a straight direction of the waveguide. We use a BEM instead of FEM because of the small wavelength resulting in a huge number of elements for far field calculations [7]. Discretizations of acoustic systems are typically done with a node distance of at least $\frac{\lambda}{10}$. For example an acoustic hemisphere of 1 m radius at a wavelength of ≈ 8.6 mm results in $4.1 \cdot 10^9$ elements. Such a huge model is not practically solvable without a computing cluster or significant reduction of the problem. In addition, we measured the properties of the measurement environment such as temperature, ambient pressure and humidity. Thus, we can implement a correct atmospheric attenuation caused by thermal conductivity, viscous and relaxation effects based on the ANSI standard S1.26-2014 [8]. A valid model of the waveguide offers the possibility to optimize the structure towards maximum sound pressure level (SPL), beam steering and also reducing of higher modes.

Our BEM model is capable of visualizing the wave propagation inside our acoustic waveguide, including a suitable prediction of the directivity pattern of the entire phased array compared to calibrated measurements.

978-1-7281-4595-2/19/$31.00 ©2019 IEEE

II. BEM Model

The main challenge of a good numeric model is a suitable accuracy which reflects the environmental properties with minimum computational load. In particular the random access memory (RAM) of a computer can be filled up quick, such as in three dimensional ultrasonic farfield calculations using FEM. One elegant way to avoid this high computational demand is the boundary element method (BEM). This numerical approach uses the surface area of a geometry instead of the volume. In comparison to an FEM, the BEM creates a dense system matrix instead of a sparse matrix. So there is a sweet spot where the complexity of an FEM exceeds a BEM. This is the case in our model.

We use a BEM implemented in COMSOL Multiphysics 5.4 (COMSOL, Sweden, Stockholm). This allows us calculating the acoustic pressure field without meshing the large air volume. The model is based on the Helmholtz equation in the frequency domain, i.e.

$$\nabla \cdot \left(-\frac{1}{\rho}\nabla p_\mathrm{t}\right) - \frac{\omega^2}{c^2\rho}p_\mathrm{t} = 0, \tag{1}$$

including the density ρ, the speed of sound c, the frequency ω and the total pressure p_t. In COMSOL the total pressure is split up into two components, i.e.

$$p_\mathrm{t} = p + p_\mathrm{b}, \tag{2}$$

which are unknown pressure p and additional harmonic background pressure p_b [8]. Our model contains no background sound field which reduces equation (2). Thermoviscous acoustics or nonlinearities are neglected as well. The geometry contains 64 independent waveguides with perpendicular input and output surfaces. The length of each channel is $80\,\mathrm{mm}$ with an input diameter of $10\,\mathrm{mm}$ and an output diameter of $3.4\,\mathrm{mm}$ (Fig. 1). The frequency is $40\,\mathrm{kHz}$ with a wavelength of $8.575\,\mathrm{mm}$ resulting in a Helmholtz number of 1.25 for the output and 3.66 for the input of the waveguide [9]. Because of the high Helmholtz number at the input, a higher acoustical mode can occur, requiring a 3D model [9]. The transducer surface is modeled as an ideal piston transducer, i.e.

$$-\mathbf{n} \cdot \left(\frac{1}{\rho\nabla p_\mathrm{t}}\right) = i\omega v_\mathrm{n}, \tag{3}$$

with a defined normal velocity v_n, applied on the inner surface at the input of the waveguide. The rigid baffle is a finite-sized sound hard wall with a thickness of $3\,\mathrm{mm}$ and a diameter of $250\,\mathrm{mm}$. All walls are assumed as ideal sound hard [Fig. 2(a)].

$$-\mathbf{n} \cdot \left(\frac{1}{\rho\nabla p_\mathrm{t}}\right) = 0. \tag{4}$$

In order to reduce calculation time, only a quarter of the geometry is simulated using the symmetric xz-plane and yz-plane [Fig. 2(b)].

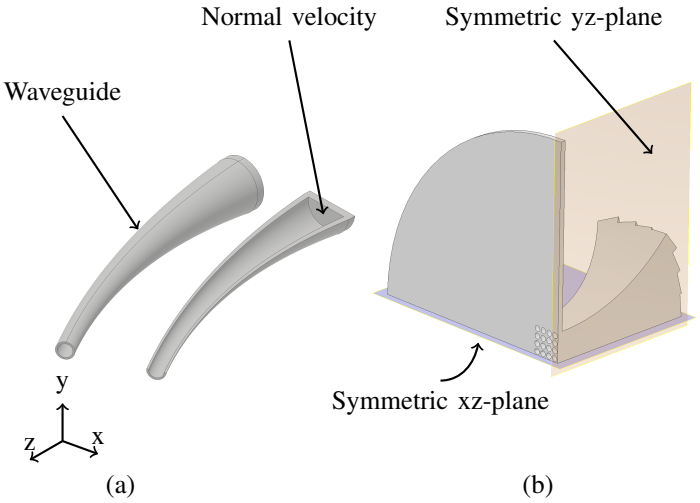

Fig. 2. A single channel of the waveguide reduces the acoustic diameter from $10\,\mathrm{mm}$ to $3.4\,\mathrm{mm}$ (a). The input and output surfaces are perpendicular to the centre line of the waveguide. The complete model exploits two symmetries at the yz-plane and at the xz-plane (b), in order to reduce calculation time.

III. Measurements

For validation measurements an ultrasonic phased array prototype of our research group was used. The phased array consists of a 3D-printed waveguide, fabricated with an Ultimaker 2 (Ultimaker BV, Geldermasen, Netherlands) using polylactic acid (PLA, Innofill PLA, Innofill 3D BV, Emmen, Netherlands). The array consists of 64 commercially available transducers (MA40S4S, Murata, Seisakusho, Nagaokakyo, Japan) each having a diameter of approximately $10\,\mathrm{mm}$. These transducers are held by an individual socket in the waveguide structure. All transducers are driven with our costum-made electronics featuring eight ultrasound pulsers (HV7355, Microship, Chandler AZ, USA), each containing eight individual channels. A field programmable gate array (FPGA) board (Zynq 7010, Xilinx, San Jose CA, USA) is used to provide the time delays for the channels. The transducers are driven with burst signals of $40\,\mathrm{kHz}$ with a cycle number of 30, reducing parasitic heating, and, thus, reducing drift of resonance frequencies. The voltage is reduced to $6\,\mathrm{V_{pp}}$ to avoid nonlinear effects in air [2].

Measurements were conducted in an anechoic chamber ($7.7\,\mathrm{m} \times 5.22\,\mathrm{m} \times 5.8\,\mathrm{m}$). The walls are covered with mineral wool cones (Grünzweig + Hartmann AG, Ludwigshafen am Rhein, Germany). With a length of $1000\,\mathrm{mm}$ and a base area of $240\,\mathrm{mm} \times 240\,\mathrm{mm}$ the cones resulting cut off frequency is $70\,\mathrm{Hz}$. Above $100\,\mathrm{Hz}$ the reflection coefficient is below 0.01 (Fig. 3).

Environmental properties were measured in the anechoic chamber using a digital pressure and temperature sensor (BMP180, Bosch GmbH, Gerlingen, Stuttgart, Germany) to validate the correct speed of sound and atmospheric attenuation used in the simulation. The temperature during measurements reached $26°\mathrm{C} \pm 0.5°\mathrm{C}$ causing a speed of sound of $347.1\,\mathrm{m/s}$ [1]. The ambient pressure was $100314\,\mathrm{hPa} \pm 1\,\mathrm{hPa}$.

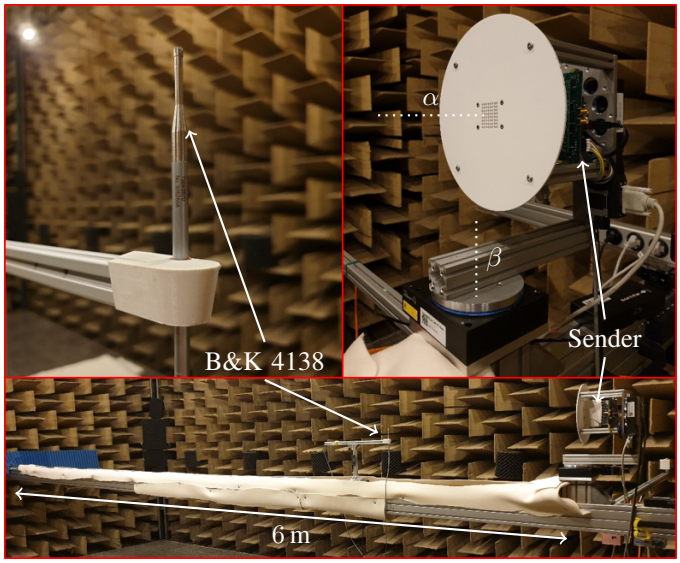

Fig. 3. The measurement setup consists of a linear axis with a calibrated measurement microphone and two rotational axes (sender location). The maximum radius is 6 m, which concludes in an effective measurement volume of up to $905\,\mathrm{m}^3$.

In addition, the humidity was measured using a DHT22 (Aosong Electronics Co.,Ltd, Guangzhou Huangpu, China) estimating additional atmospheric damping effects. The value used is $39\% \pm 2\%$ RH.

The measurement system contains of three movable axes. Two rotational ones (M-061.2S and M-062.2S, Physik Instrumente, Karlsruhe, Germany) are used to rotate the sender in plane orientation to the receiver (microphone). The accuracy of both axes are suitable for this measurement purpose with $\pm 0.0011°$ for the β-axis and $\pm 0.00051°$ for the α-axis. A calibrated measurement microphone (Type 4138, Brüel & Kjaer, Naerum, Denmark) is mounted on a 6-m linear axis (LEFZ 1, Isel Automation, Eichenzell, Germany) featuring an accuracy of ± 0.2 mm. The microphone is tilted $90°$ to reduce the directivity of the receiver [10]. The microphone signal is analyzed by a data acquisition system (NI PXI-5922, National Instruments, Austin, TX, USA) with 500 kSa. The entire system is controlled with a PC using LabVIEW (National Instruments, Austin, TX, USA) [2]. All measurement setup features a noise floor of 60 dB and a maximum SPL of 171 dB, limited by the microphone, resulting in a dynamic range of 110 dB. By using a meander structure in polar coordinates, the system allows two measurement points per second (Fig. 3).

The phased array is used as an far field array. The ideal far field characteristic reduces the signal amplitude with $\frac{1}{r}$ where r is the distance between the acoustic source and an arbitrary point in the far field. Following the far field criteria

$$N = \frac{D^2 - \lambda^2}{4\lambda} \tag{5}$$

the transition between near and far field is around 30 mm [1]. Measuring a distance more than 1 m just increases the measurement and simulation time without any improvements regarding the results, i.e. only up to 1 m measurements are performed.

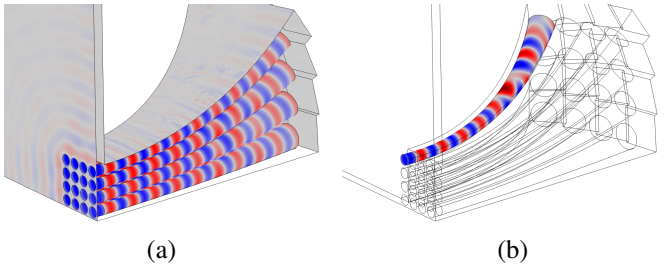

Fig. 4. The simulation result shows an almost ideal plane wave propagation within the waveguide (a). The corner channels deviate the strongest from plane wave propagation (b).

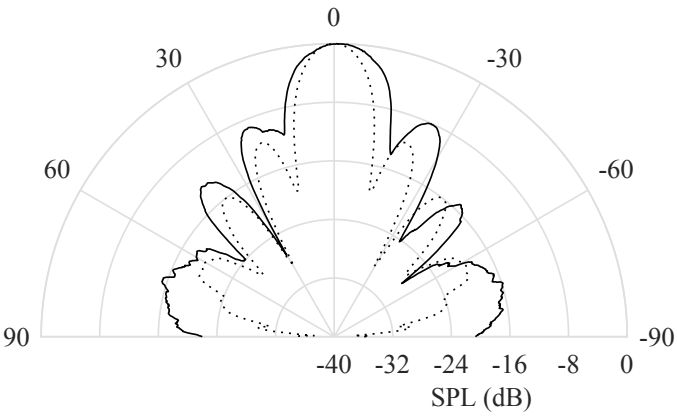

Fig. 5. The BEM (:) is in good agreement with the measurement (-). The main lobe differs only $4°$. Due to the amplitude deviation of the used transducers, the side lobes differ from the simulation.

IV. Results and Discussion

The propagation inside the waveguide system shows that most of the ducts result in a plane wave propagation [Fig. 4(a)]. However, the corner element creates a curved wave front [Fig. 4(b)]. This can be explained by the bending angle of the duct. In addition, the diameter of the input section of the duct is capable of supporting higher modes as well. So the direction of propagation has an influence on the system.

To compare the directivity between measurement and simulation, both graphs are normalized to their respective maximum SPL. The BEM model creates a directivity pattern which is in good agreement with our measurements (Fig. 5). The half power beam width just differs by $4°$ and the side lobe level by 3 dB. The side lobes show slightly different behaviour caused by the amplitude deviation of the transducers used. This deviation is not considered in the model. The side lobes between $\pm 60°$ and $\pm 90°$ show in both measurement and BEM model a more rippled distribution. This effect is caused by the finite-sized rigid baffle. The finite-sized sound-hard wall results in an abrupt change in acoustic impedance, creating additional reflections of the sound wave along the rigid baffle.

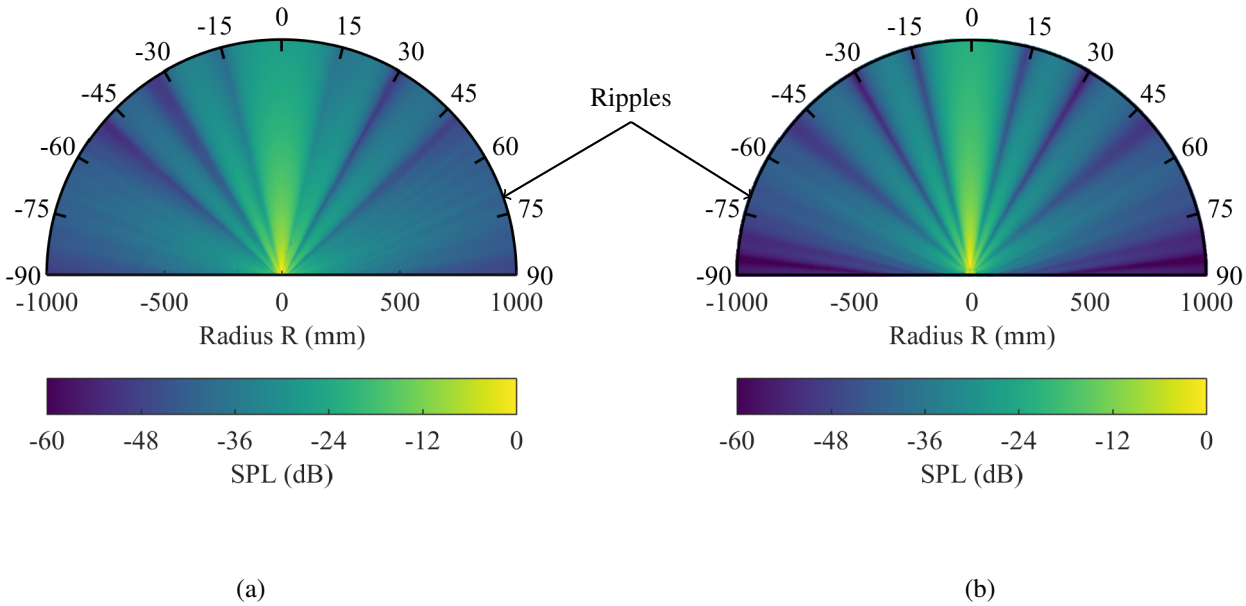

Fig. 6. The measurement (a) and the BEM simulation (b) show a similar pressure distribution. The transition between the lobes, e.g. at $\pm 15°$ in the measurement, are not as sharp as in the simulation due to the amplitude deviation of the transducers used. In both graphs the influence of the finite-sized rigid baffle is noticeable in the third side lobe (ripples).

The calculated and measured 2D SPL distribution are in good agreement. However, the influence of the transducer manufacturer tolerances are noticeable. The main lobe directs in the same orientation and there is a small difference between the half power beam widths of $4°$. The first side lobe highlights a sharp borderline from the main lobe. This transition is not as sharp as in the measurement due to the different amplitudes of the transducers at $\pm 15°$ [Fig. 6(a)]. When each transducer emits a sound wave with a different amplitude, the destructive interferences of the propagating waves are not ideal causing a much higher resulting pressure at this point. The second side lobe is in a good agreement with the measurement. The last side lobe contains ripples [Fig. 6(b)]. This is caused due to the finite-sized rigid baffle. At the edge of the baffle an abrupt change in impedance exists, which leads to some reflections on the surface of the rigid baffle. These reflections intersect with the incident waves and create this pressure distribution.

V. CONCLUSION

This work shows that our BEM model estimates the directivity pattern of the ultrasonic phased array accurately with only small differences. The calculations can be done on a single CPU server with no need for calculation clusters. The far field characteristics of the calibrated measurements are in good agreement with the simulations. The differences concerning the half power beam widths is only $4°$ and for the side lobe level 3 dB. The influence of the finite-sized rigid baffle is noticeable, resulting in additional ripples in the pressure distribution at the third side lobes. The amplitude variation of each transducer is not implemented in the model, causing a minor difference in side lobe characteristics.

Our next step is to combine BEM and FEM to benefit from both numerical methods, in order to decrease the numerical cost so that there is no need for using symmetric planes.Then we can demonstrate the beam steering of the main lobe in the simulation, as well.

ACKNOWLEDGMENT

This work received funding from Pepperl+Fuchs AG, Mannheim, Germany.

REFERENCES

[1] R. Lerch, G. Sessler, and D. Wolf, *Technische Akustik: Grundlagen und Anwendungen*. Springer, 2009.
[2] A. Jäger, D. Großkurth, M. Rutsch, A. Unger, R. Golinske, H. Wang, S. Dixon, K. Hofmann, and M. Kupnik, "Air-coupled 40-khz ultrasonic 2d-phased array based on a 3d-printed waveguide structure," in *2017 IEEE International Ultrasonics Symposium (IUS)*, pp. 1–4, Sep. 2017.
[3] A. Langen, "Ein verfahren zur konstruktion anwendungsoptimierter ultraschallsensoren auf der basis von schallkanalen," Ph.D. dissertation, Universität Stuttgart, 1993.
[4] S. J. Takayuki Takahashi, Ryosuke Takahashi, "Ultrasonic phased array sensor for electric travel aids for visually impaired people," in *ICMIT 2007: Mechatronics, MEMS, and Smart Materials*, vol. 6794, 2008.
[5] R. Golinske, M. Hoffmann, E. Konetzke, A. Unger, M. Rutsch, and M. Kupnik, "Diffraction loss calculation based on boundary element method for an air-coupled phased array," in *2015 IEEE International Ultrasonics Symposium (IUS)*, pp. 1–4, Oct 2015.
[6] S. T. Shigeru Igarashi, "Control of ultrasonic acoustic fields by multiple acoustic waveguides and piezoelectric transducers," in *The Fifth International Conference on Sensor Device Technologies and Applications*, 2014.
[7] R. BOLEJKO and A. DOBRUCKI, "Fem amd bem computing costs for acoustical problems," *Archives of Acoustics*, vol. 31, no. 2, 2014.
[8] *Acoustics Module User's Guide*, COMSOL, 2018.
[9] F. Fahy and T. D. Rossing, "Foundations of engineering acoustics," *Journal of The Acoustical Society of America*, vol. 111, pp. 1142–1142, 2002.
[10] *Datasheet 1/8" Pressure-field Microphone Type 4138*, Brüel & Kjaer, 2008.